Joule

CellPress

Article

Next-generation thermoelectric cooling modules based on high-performance $Mg_3(Bi,Sb)_2$ material

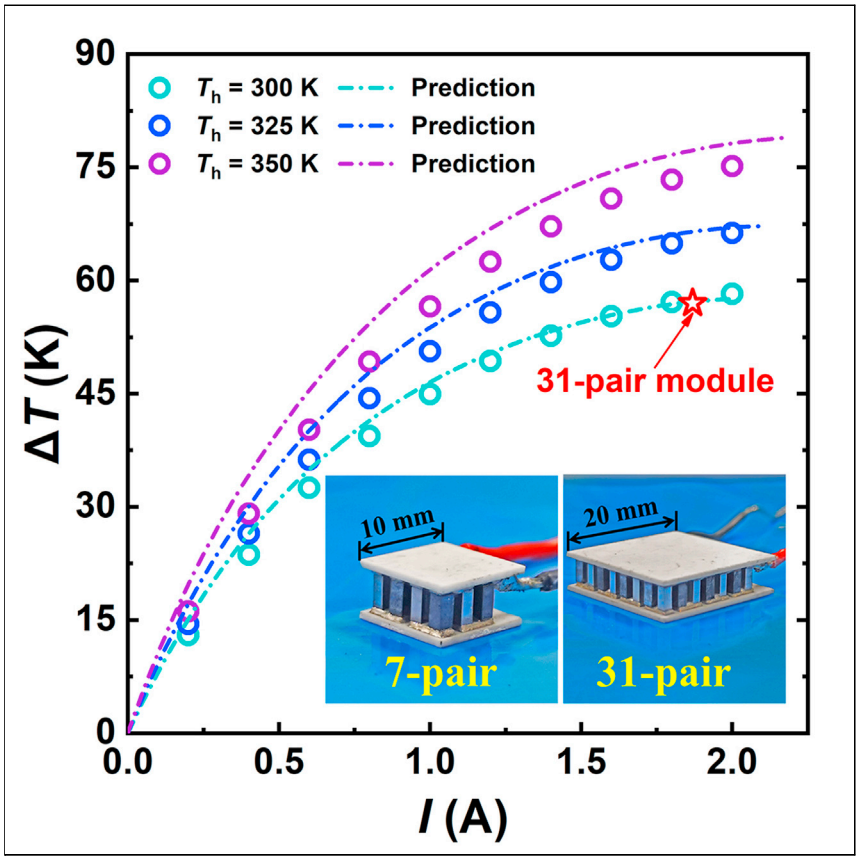

Full-scale thermoelectric cooling modules (7, 31, and 71 pairs) based on n-type $Mg_{3.2}Bi_{1.4975}Sb_{0.5}Te_{0.0025}$ and p-type $(Sb_{0.75}Bi_{0.25})_2(Te_{0.97}Se_{0.03})_3$ have been successfully fabricated in our work. Enhanced stability of $Mg_3(Bi,Sb)_2$ material was realized by introducing a hot deformation process, and meanwhile highly reliable Mg_2Cu contact layer to $Mg_3(Bi,Sb)_2$ material was developed. The superior thermoelectric cooling performance and service durability were achieved in our module, a striking benefit of 23% higher performance-cost ratio over commercial Bi_2Te_3 enables it the promising candidate for next-generation thermoelectric cooling.

Jiawei Yang, Guodong Li, Hangtian Zhu, ..., Yuan Yao, Ronggui Yang, Huaizhou Zhao

htzhu@iphy.ac.cn (H.Z.)
hzhao@iphy.ac.cn (H.Z.)

Highlights

A highly reliable Mg_2Cu contact layer is developed for $Mg_3(Bi,Sb)_2$

Full-scale cooling modules based on high-performance $Mg_3(Bi,Sb)_2$ have been realized

A maximum ΔT of 76 K with the hot-side temperature of 350 K was achieved

The striking benefit lies in its high-performance cost ratio over Bi_2Te_3 modules

Yang et al., Joule 6, 1–12
January 19, 2022
https://doi.org/10.1016/j.joule.2021.11.008

Please cite this article in press as: Yang et al., Next-generation thermoelectric cooling modules based on high-performance $Mg_3(Bi,Sb)_2$ material, Joule (2021), https://doi.org/10.1016/j.joule.2021.11.008

Joule

CellPress

Article

Next-generation thermoelectric cooling modules based on high-performance $Mg_3(Bi,Sb)_2$ material

Jiawei Yang,[1,2] Guodong Li,[1] Hangtian Zhu,[1,*] Nan Chen,[1,2] Tianbo Lu,[1] Junling Gao,[1] Liwei Guo,[1] Junsen Xiang,[1] Peijie Sun,[1] Yuan Yao,[1] Ronggui Yang,[3] and Huaizhou Zhao[1,4,*]

SUMMARY

As the core component of any real thermoelectric cooling system, the Bi_2Te_3-based modules have been used for decades. Recently, n-type $Mg_3(Bi,Sb)_2$ material was proposed as a promising substitute for Bi_2Te_3. However, the fabrication of commercially viable modules with such new materials is challenging. Herein, full-scale cooling modules based on the optimized n-type $Mg_{3.2}Bi_{1.4975}Sb_{0.5}Te_{0.0025}$ and p-type $(Sb_{0.75}Bi_{0.25})_2(Te_{0.97}Se_{0.03})_3$ were successfully fabricated. A maximum ΔT of 76 K with the hot-side temperature of 350 K, a COP of 8 with a temperature difference of 5 K, and a serving time >6 months were achieved. These were attributed to the enhanced stability and well-secured n-type transport of the $Mg_{3.2}Bi_{1.4975}Sb_{0.5}Te_{0.0025}$, a highly reliable Mg_2Cu barrier layer, and other key techniques involved in the module assembling. The most striking benefit of our modules lies in its 23% higher performance-cost ratio over commercial Bi_2Te_3 system, which paves its way for next-generation thermoelectric cooling applications.

INTRODUCTION

Thermoelectric modules, capable of energy conversion between heat and electricity, have long been used for effective all-solid cooling and waste heat recovery. The efficiency of these modules is usually estimated by a dimensionless zT value of thermoelectric materials, $zT = S^2\sigma T/(\kappa_l + \kappa_e)$, where S is the Seebeck coefficient, σ is the electrical conductivity, T is the temperature, and κ_l and κ_e are the lattice and electron thermal conductivities, respectively. Therefore, to enable the broad use of these modules in commercial and other critical fields, enormous efforts have been devoted to improving the zT value of materials, mainly by enhancing power factor ($S^2\sigma$) through the engineering of electronic structures[1–5] and charge carrier scattering[6–8] and reducing lattice thermal conductivity (κ_l) by designing soft materials with complex crystal structures[9–13] or enhanced phonon scattering.[10,14–19] However, the actual performance of thermoelectric modules cannot be predicted simply from the zT values of materials because it is governed by a variety of properties, including average thermoelectric properties,[20] mechanical properties,[21] thermal and chemical stabilities,[22,23] interfacial contact, and thermal resistances related to the barrier layers.[24,25]

The most important commercial application of thermoelectricity is near room temperature cooling,[26] and Bi_2Te_3-based modules are currently the only industrial choice for such purpose with maximum cooling temperature difference of 60–70 K. Although many new materials with superior thermoelectric properties at near room temperature have been identified in recent years[27,28] and various new mechanisms for zT enhancement have been recognized,[29] their impact on the near room temperature cooling

Context & scale

For half a century, the Bi_2Te_3-based modules, at the cost of large consumption of Te sources, have been the only commercial device for near room temperature thermoelectric cooling. Herein, we have fabricated the full-scale cooling modules based on n-type $Mg_{3.2}Bi_{1.4975}Sb_{0.5}Te_{0.0025}$ and p-type $(Sb_{0.75}Bi_{0.25})_2(Te_{0.97}Se_{0.03})_3$. A maximum cooling temperature (ΔT_{max} of 76 K), maximum efficiency of performance (COP of 8), and a long-serving time lasting more than 6 months were realized for the modules. Attractively, the cooling performance and durability of the modules are comparable with those of the commercial Bi_2Te_3-based modules with a ~23% enhancement on the performance-cost ratio. The keys are attributed to the highly reliable barrier layer of Mg_2Cu, the enhanced stability and durability of the n-type transport behavior in $Mg_{3.2}Bi_{1.4975}Sb_{0.5}Te_{0.0025}$, as well as other key techniques involved in the module assembling procedure.

application remains unclear. The main reason for this gap is the lack of performance verification through full-scale modules that are based on these new materials. A full-scale thermoelectric module consists of n- and p-type material legs that are connected electrically in series and thermally in parallel. Such a module can provide sufficient cooling density and output power for practical applications. Therefore, thermoelectric properties and the service durability of new materials need to be further confirmed via fabrication and performance evaluation of full-scale module.[22,30,31]

As a new material system, n-type $Mg_3(Bi,Sb)_2$ has become one of the focuses of thermoelectric research and undergone rapid improvement in terms of its zT values, especially at room temperature.[32–36] Fundamentally, thermoelectric performance of this material can be optimized by tuning the band structure and carrier concentration for the purpose of applications at different temperatures.[37–39] Manipulation of the scattering mechanism has been identified as an effective approach to increase the carrier mobility in $Mg_3(Bi,Sb)_2$ systems.[6,8,37] In the particular instance, the electrical transport properties at near room temperature can be significantly improved through the reduction of grain boundary scattering of electrons in $Mg_3(Bi,Sb)_2$.[8,40–42] The power factor of single crystal sample with composition of $Mg_3Bi_{1.25}Sb_{0.75}$ reaches 41 $\mu W\,cm^{-1}\,K^{-2}$ at room temperature,[40] and the room temperature zT of up to 0.8 has been both achieved in annealed bulk $Mg_{3.01}Sb_{1.49}Bi_{0.5}Te_{0.01}$ and above single crystal samples,[40,42] which are very close to those of the industrially available n-type Bi_2Te_3 ($zT = 0.85$, $S^2\sigma = 40\ \mu W\,cm^{-1}\,K^{-2}$) (Figure S1), indicating the potential of this material system in refrigeration applications.

Regardless of the rapidly improving performance of n-type $Mg_3(Bi,Sb)_2$ and its promising prospect, its stability as a Zintl phase material and performance in full-scale modules remain unsettled.[22,24] Though the cooling performance of $Mg_3(Bi,Sb)_2/Bi_2Te_3$ unicouple prototype has been demonstrated by Mao et al.,[33] an applicable full-scale module with the cooling performance that is consistent with the thermoelectric properties of materials is yet to be achieved.[43] A prototype unicouple device is too limited to provide the cooling capacity, durability, and other key parameters that a commercially viable full-scale cooling module could offer. However, there are two main challenges in the fabrication of the full-scale cooling module based on $Mg_3(Bi,Sb)_2$ materials. First, instead of the high zT values, the thermal stability and durability of the thermoelectric performance of $Mg_3(Bi,Sb)_2$ is of paramount interest, as it could severely hinder its application in cooling modules. Second, the interfacial materials: why the Ni/Fe electrode is not appropriate for the fabrication of full-scale cooling modules of $Mg_3(Bi,Sb)_2$? How could we prevent the deterioration of thermoelectric performance of the $Mg_3(Bi,Sb)_2$ material during the hot pressing of the electrode at high temperatures? In this work, the detrimental transition from n-type to p-type electrical transport behavior can be prominently restrained in $Mg_{3.2}Bi_{1.4975}Sb_{0.5}Te_{0.0025}$ material owing to the suppression of Mg-deficient grain boundary phases through the post hot deformation process. Based on this material, full-scale cooling modules (with 7, 31, and 71 pairs), comprising a hybrid n-type $Mg_{3.2}Bi_{1.4975}Sb_{0.5}Te_{0.0025}$ and a p-type $(Sb_{0.75}Bi_{0.25})_2(Te_{0.97}Se_{0.03})_3$ (MBST/SBTS), were fabricated using the highly reliable Mg_2Cu as the barrier layer. For the 7-pair cooling module, we achieved a maximum cooling temperature of 76 K with a hot-side temperature of 350 K and a maximum coefficient of performance (COP) of 8 with a temperature difference of 5 K. The high cooling performance could also be realized in the 31-pair module, and the measured result is well reproduced by a third party (Figure S2). The resistance of the test module only increased by 5% after working under the optimized current of 3 A for 3,000 min, and after that the cooling performance remained stable for at least 6 months, thereby demonstrating the module's high reliability. Overall, the functionalities of the $Mg_3(Bi,Sb)_2$-based

[1]Beijing National Laboratory for Condensed Matter Physics, Institute of Physics, Chinese Academy of Sciences, Beijing 100190, China

[2]School of Physical Sciences, University of Chinese Academy of Sciences, Beijing 100049, China

[3]School of Energy and Power Engineering, Huazhong University of Science and Technology, Wuhan, Hubei 430074, China

[4]Lead contact

*Correspondence: htzhu@iphy.ac.cn (H.Z.), hzhao@iphy.ac.cn (H.Z.)

https://doi.org/10.1016/j.joule.2021.11.008

Please cite this article in press as: Yang et al., Next-generation thermoelectric cooling modules based on high-performance $Mg_3(Bi,Sb)_2$ material, Joule (2021), https://doi.org/10.1016/j.joule.2021.11.008

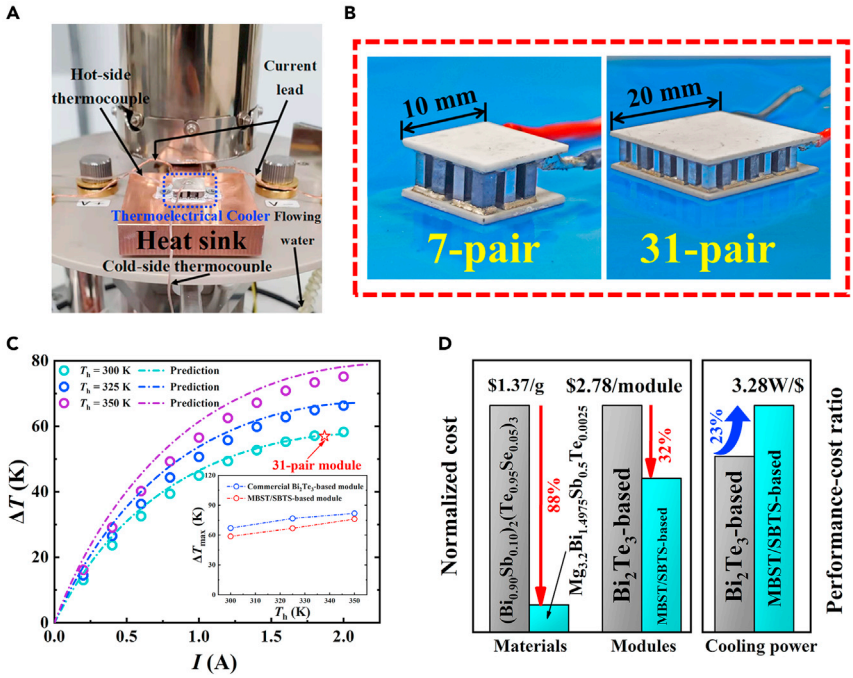

Figure 1. Performance of full-scale MBST/SBTS cooling modules

(A and B) (A) The measuring equipment for ΔT and (B) the as-fabricated full-scale MBST/SBTS cooling modules.

(C) Measured ΔT as a function of the input electric current for a 7-pair cooling module with a leg height of 3 mm. The dotted-dashed lines represent the theoretical predictions based on an analytical model. A comparison of the maximum ΔT between our module and the commercial Bi_2Te_3-based module is shown in the inset figure.

(D) Normalized cost for the two types of materials and corresponding modules, and the performance-cost ratio of cooling power for two kinds of modules.

cooling module are comparable to that of the modules made of commercial Bi_2Te_3 (Figures S1 and S3). The most striking advantage, from the perspective of low material cost and high cooling power of the MBST/SBTS module, lies in its 23% higher performance-cost ratio over commercial Bi_2Te_3-based module.

RESULTS AND DISCUSSION

The most efficient way to evaluate the cooling performance of a thermoelectric module is to measure the maximum cooling temperature (ΔT_{max}) between its two sides that could be produced under zero cooling loads. Figure 1 summarizes our measurement setup and the performance of our full-scale MBST/SBTS cooling modules (Figure 1B). As the current passes through, a temperature difference (ΔT) between the cold (T_c) and hot sides (T_h) of the module is created because of the Peltier effect. As the current increases with zero heat load, the Peltier effect (related to S) approaches a balance with Joule heat inside the materials (related to σ) and heat conduction due to the temperature gradient (associated with κ); then, ΔT can reach the maximum value $\Delta T_{max} = 1/2\ z_d\ T_c^2$, where z_d represents the z value of the device.[29] Compared with the recently reported recorded high room temperature zT value of ~0.8 for $Mg_3(Bi,Sb)_2$ materials,[40,42,44] the zT value in this work reached 0.7 (Figure S1). The MBST/SBTS modules prepared herein generated a series of ΔT_{max} close to that of the commercial Bi_2Te_3-based module (Figure 1C). The measured ΔT_{max} of 7-pair module increased from 59 K (hot-side temperature = 300 K) to 76 K (hot-side temperature = 350 K), thereby showing consistency with the theoretical simulations

Please cite this article in press as: Yang et al., Next-generation thermoelectric cooling modules based on high-performance $Mg_3(Bi,Sb)_2$ material, Joule (2021), https://doi.org/10.1016/j.joule.2021.11.008

under an analytical model (see supplemental information for more details). An identical ΔT_{max} of 57 K can also be produced by the 31-pair module (at hot-side temperature of 300 K), which confirms the reliable design and fabrication technique developed in this work (Figure 1C). It is worth mentioning that the cooling performance of 31-pair module has been verified by a third party with the same ΔT_{max} value of 57 K obtained (Figure S2). Notably, the maximum ΔT of our module is only slightly lower (12%) than that of commercial Bi_2Te_3-based modules, as indicated by the inset of Figure 1C. The contact resistance of the n- and p-type legs and the geometry and thermal conductivity of Al_2O_3 plates were considered in the calculation to enable the physical description of a real module. However, the small deviation between the measurement and simulation results could be attributed to the reasonable ignoring of the thermal resistance of the interfaces.

Most importantly, from the application point of view, except for the special cares paid to the preparation and manufacturing of $Mg_{3.2}Bi_{1.4975}Sb_{0.5}Te_{0.0025}$ material and thermoelectric legs, most other fabrication methods are traditional and common, and highly compatible with the manufacturing of commercial Bi_2Te_3 modules. This would be a great benefit for the production of $Mg_3(Bi,Sb)_2$ based modules, as the industry would prefer to adopt this new material without many changes to their techniques. Based on these merits, we can rationally estimate the cost of our modules. Considering that the raw materials are the relatively stable investment in the whole manufacturing process, while the cost of manufacturing would depend on the continuing advances of the involved technologies, we use the prevailing investment in manufacturing from two industrial sources to calculate the total cost of our module with 31 pairs. Because of the avoided use of rare element Te (Table S1), the $Mg_{3.2}Bi_{1.4975}Sb_{0.5}Te_{0.0025}$ presents a significant reduction of cost on basis of materials (88% lower), and in turn the 32% lower cost of the cooling module over Bi_2Te_3-based commercial module (Figure 1D in the left). The performance-cost ratio of the cooling module is evaluated by dividing the maximum heating flow at ΔT = 0 by the cost of the module. Considering the high cooling power in MBST/SBTS cooling modules, a 23% higher performance-cost ratio (Figure 1D in the right) over commercial Bi_2Te_3-based module is achieved. Thus, the slightly higher cooling performance of the commercial Bi_2Te_3-based module (Figure 1C) over our modules would concede to the significant performance-cost ratio increase of 23% in MBST/SBTS modules in the case of real applications. In the future study, some low-cost high-performance p-type thermoelectric materials, such as SnSe[45] and skutterudite,[46] can be used as the possible substitute for p-type Bi_2Te_3 to realize non-Bi_2Te_3-based thermoelectric cooling modules thus would completely avoid the use of Te and further reduce the cost of thermoelectric cooling.

Despite of the n-type $Mg_{3.2}Bi_{1.4975}Sb_{0.5}Te_{0.0025}$ material we used in the MBST/SBTS modules, other compositions of $Mg_{3.2}Bi_xSb_{2-x}$ might be also suitable for room cooling application. The Bi-rich $Mg_{3.2}Bi_xSb_{2-x}$ alloy is believed to possess favorable near room temperature thermoelectric performance owing to the smaller effective mass and reduced lattice thermal conductivity.[38] However, due to the narrow band gap and the strong bipolar effect of $Mg_{3.2}Bi_2$, the optimal compositions for thermoelectric cooling applications are roughly located in the range of $1.2 \geq x \geq 1.75$ for Bi, which is confirmed by the theoretical predictions based on SPB model and literature reports in Figure 2A (see supplemental information for more details) and Figure S4.[33,37,47] The corresponding room temperature ΔT_{max} of the modules based on the n-type $Mg_{3.2}Bi_xSb_{2-x}$ materials in Figure S4 and p-type commercial $(Sb_{0.75}Bi_{0.25})_2(Te_{0.97}Se_{0.03})_3$ can be estimated as shown in Figure 2B, where the same contact resistivity as being measured in this work was used in these calculations. The peak values of ΔT_{max} (55–60 K) were observed to locate at the same

Please cite this article in press as: Yang et al., Next-generation thermoelectric cooling modules based on high-performance $Mg_3(Bi,Sb)_2$ material, Joule (2021), https://doi.org/10.1016/j.joule.2021.11.008

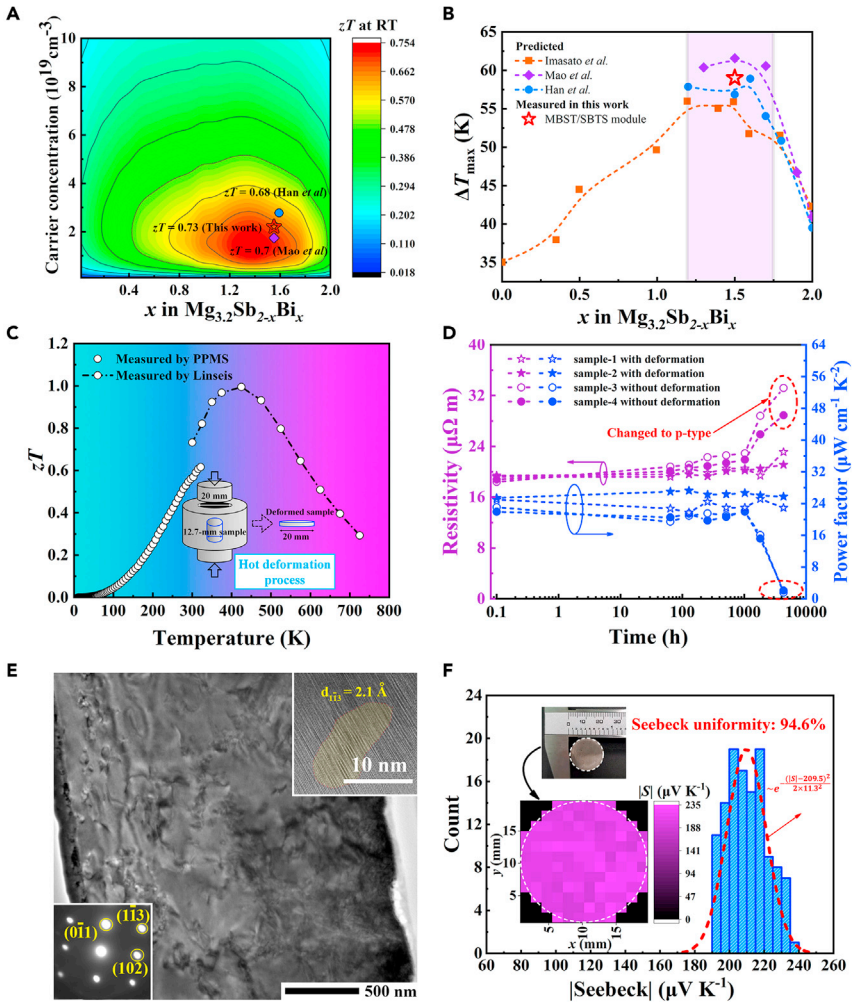

Figure 2. Preparation and characterization of the $Mg_{3.2}Bi_{1.4975}Sb_{0.5}Te_{0.0025}$ material with optimal thermoelectric performance and durability

(A) The carrier concentration and composition dependent zT values at 300 K for $Mg_{3.2}Bi_xSb_{2-x}$ materials from theoretical predictions and literature reports.

(B) The predicted ΔT_{max} of the MBST/SBTS modules based on these materials in (Figure 2A), where the commercial $(Sb_{0.75}Bi_{0.25})_2(Te_{0.97}Se_{0.03})_3$ was used as p-type counterpart leg in these modules.

(C) zT value of $Mg_{3.2}Bi_{1.4975}Sb_{0.5}Te_{0.0025}$ sample prepared using the hot deformation process. Schematic of the hot deformation process is shown in the inset of Figure 2C.

(D) Aging time dependence of electrical transport properties for samples with and without the hot deformation process.

(E) TEM images of the hot-deformed samples with a rich variety of defects. Scale bars for low and high (inset) magnification TEM images represent 500 nm and 10 nm, respectively.

(F) Distribution of Seebeck coefficient across the 20-mm diameter disk samples.

optimal range of $1.2 \geq x \geq 1.75$ for $Mg_{3.2}Bi_xSb_{2-x}$. Therefore, we use the representative $Mg_{3.2}Bi_{1.4975}Sb_{0.5}Te_{0.0025}$ composition (carrier concentration 2×10^{19} cm^{-3}; Figure S5) in this work to evaluate and enhance its thermal stability and durability for the fabrication of full-scale high-performance thermoelectric cooling modules.

To obtain a deeper understanding of the material properties of $Mg_{3.2}Bi_{1.4975}Sb_{0.5}Te_{0.0025}$ and the mechanisms related to its service abilities, we characterized its transport properties in a wide temperature range (~10 to 725 K). The results are shown in Figures 2C and

Please cite this article in press as: Yang et al., Next-generation thermoelectric cooling modules based on high-performance $Mg_3(Bi,Sb)_2$ material, Joule (2021), https://doi.org/10.1016/j.joule.2021.11.008

S1. The zT of the as-prepared $Mg_{3.2}Bi_{1.4975}Sb_{0.5}Te_{0.0025}$ sample at room temperature was 0.7 (slightly lower than that of the commercial n-type $(Bi_{0.90}Sb_{0.10})_2(Te_{0.95}Se_{0.05})_3$, i.e., 0.85), and it reached the peak value of 1.0 at 420 K, which was >10% higher than that of $(Bi_{0.90}Sb_{0.10})_2(Te_{0.95}Se_{0.05})_3$, i.e., 0.9. Meanwhile, $Mg_3(Bi,Sb)_2$-based thermoelectric materials have been reported by many groups and exhibited higher zTs at higher temperature for power generation applications.[35,36] Our value of ~0.7 at room temperature is one of the highest and better for cooling modules, as has been proved by the significant ΔT_{max} value of 59 K achieved in MBST/SBTS modules (Figure 1C).

Despite the superior thermoelectric properties of n-type $Mg_3(Bi,Sb)_2$-based materials, the durability or service stability of such materials remains a critical concern in cooling modules.[22,24] For example, by continuously monitoring the thermoelectric properties of hot-pressed samples for 6 months, we found that the resistivity began to increase abruptly at 100 h after the synthesis of the sample and eventually resulted in the change of transport behavior to p-type with the power factor close to zero (Figure 2D). It is believed that a Mg-deficient grain boundary phase would gradually accumulate, thus inducing increasingly strengthened electron scattering and dramatically reducing the room temperature mobility of the carrier[8,48,49] (Figure S5). As the Mg-deficient grain boundary phase grows, strong bipolar effect stemming from the increased hole concentration would completely deteriorate the n-type feature and lead to a poor p-type dominated thermoelectric performance with a positive Seebeck coefficient value of ~70 $\mu V\ K^{-1}$.

In this work, following the conventional ball-milling and hot pressing process, we introduced a post hot deformation process. Previous study revealed that the loss of Mg in the $Mg_3(Bi,Sb)_2$ materials is the main cause of performance degradation in the sample. Excess Mg is widely used to suppress the formation of Mg vacancies to secure the n-type transport behavior and also to improve the stability for $Mg_3(Bi,Sb)_2$.[48] In this work, the initial purpose of post hot deformation was to improve the uniformity of the samples. As shown in Figure S6, the large cluster of Mg-rich phase (~3 μm) in the hot-pressed sample can be further pulverized to small pieces during hot deformation, leading to uniform distribution of excess Mg in the samples. In addition, the dislocation and other defects in the hot-deformed sample, as shown in Figure 2E, can significantly promote the diffusion rate of Mg atoms by orders of magnitude, as reported in other systems.[50,51] More specifically, according to Fick's first law, Mg atomic flux in the materials is determined by $J = -D\nabla c$, where D is diffusion coefficient, ∇c is concentration gradient of Mg element. Assuming the net loss of Mg remains constant, then the diffusion flux J is constant. Considering that the deformation process can significantly promote D, the ∇c in the sample will be reduced, thus maintaining a uniform chemical potential for the Mg-rich samples. The uniform phase and elemental distributions in a hot-deformed sample can secure much durable n-type thermoelectric performance compared with the hot-pressed sample. Surprisingly, as shown in Figure 2D, the power factor of the sample had no visible degradation even after 6 months of monitoring in ambient conditions. Furthermore, we checked and characterized the uniformity of the hot-deformed sample. As shown in Figure 2F, we chose to map the distribution of the Seebeck coefficients; this coefficient is the most sensitive parameter governing thermoelectric performance. The 20-mm pellet was marked into 120 regions, and the Seebeck coefficient of each region was measured to be ~210 $\mu V\ K^{-1}$ and evenly distributed over the whole area of the sample. According to the statistical calculation, the uniformity of the Seebeck coefficients was 94.6% (Figures 2F and S7). As a result, the 20-mm pellets with stable, uniform distribution of high thermoelectric properties would lay the basis for the mass production of $Mg_{3.2}Bi_{1.4975}Sb_{0.5}Te_{0.0025}$

and fabrication of high-performance cooling modules.[52] The post hot deformation process developed in this work, simple but effective, truly triggers the transformation of $Mg_3(Sb,Bi)_2$ from material study to real device applications.

In the fabrication of $Mg_3(Bi,Sb)_2$-based cooling modules, suitable diffusion barrier materials should possess good chemical stability, similar coefficients of thermal expansion (CTE) values, strong bonding strength, low contact resistance, and relatively low processing temperature to prevent the property degradation of $Mg_3(Bi,Sb)_2$. Recently, Fe and Ni metal layers prepared by one-step powder sintering have been verified to be the suitable electrical contact layers for $Mg_3(Bi,Sb)_2$ leg.[24,33] However, heat treatment of the pellet $Mg_3(Bi,Sb)_2$ sample at high temperatures (close to the melting temperature of Ni of 1,728 K) by hot pressing Ni electrode would lead to the severe deterioration of the thermoelectric performance of the material. In addition, it is often difficult to obtain a uniform and thin contact layer by hot pressing multiple layers of powders (including $Mg_3(Bi,Sb)_2$ material powder and Ni/Fe powder) during the mass production process of real thermoelectric legs (usually with the height of 1–2.5 mm in commercial products), as the layers tend to deform and mix under pressure. This makes a great challenge in the fabrication of high-quality $Mg_3(Bi,Sb)_2$-based legs and full-scale cooling modules by using Ni/Fe electrodes. In contrast to Ni/Fe electrode, Mg_2Cu was identified as a suitable barrier layer for $Mg_3(Sb,Bi)_2$ materials (Figure S8). As can be seen from the ternary phase diagram of Cu-Mg-Sb(Bi) (Figures 3A, 3B, and S9), Mg_2Cu is thermodynamically stable in the phase region of Mg-Mg_2Cu-$Mg_3Bi_{1.5}Sb_{0.5}$, new phases cannot form at the interface of $Mg_2Cu/Mg_3Bi_{1.5}Sb_{0.5}$ even at near room temperature. Thus, the diffusion of Cu into $Mg_3(Sb,Bi)_2$ can be effectively avoided, which secures the high thermoelectric performance of $Mg_3(Sb,Bi)_2$. Indeed, as shown in Figure S10, the Mg_2Cu is more reliable than Fe as the barrier layer for $Mg_3(Sb,Bi)_2$. Meanwhile, Mg_2Cu has a low melting point (853 K) and can be facilely post hot-pressed to the $Mg_3(Sb,Bi)_2$ pellet samples at as low as 803 K without sacrificing the thermoelectric properties of the sample.

Herein, a multilayer structure of $Cu/Mg_2Cu/Mg_{3.2}Bi_{1.4975}Sb_{0.5}Te_{0.0025}$ was designed to provide a stable contact for the cooling module. To prepare the contact layer with uniform thickness for mass production, we used Cu foil, Mg_2Cu powder, and $Mg_{3.2}Bi_{1.4975}Sb_{0.5}Te_{0.0025}$ pellet as starting materials for the sintering process (Figure S11). As only Mg_2Cu was in powder form, a uniform contact layer with a clear boundary between $Mg_{3.2}Bi_{1.4975}Sb_{0.5}Te_{0.0025}$ and Mg_2Cu were formed (as shown in the inset of Figures 3C and S12). The diffusion region of Cu at the boundary after hot pressing was quantified using energy dispersive X-ray spectrometry (EDS) (Figures 3C and S13). Based on the elemental mapping, the thickness of the diffusion layer was calculated to be ~0.428 μm by fitting the curve of Cu distribution (See supplemental information for additional discussion), which is consistent with the scanning electron microscopy (SEM) images. The thin diffusion layer formed during the sintering process indicated good chemical and thermal stability between the Zintl phase $Mg_{3.2}Bi_{1.4975}Sb_{0.5}Te_{0.0025}$ and the barrier material Mg_2Cu. The electrical contact resistivity (ρ_c) of the $Mg_{3.2}Bi_{1.4975}Sb_{0.5}Te_{0.0025}$ leg was estimated to be as low as 12 $\mu\Omega$ cm^2 using four-probe method[24] (Figure 3D). The contact resistance of both sides of the n-type leg contributed to only 3.8% of the total resistance of the 3-mm n-type leg, which remained stable for 6 months and even longer.

As thermal stress is unavoidable because of the temperature gradient generated during the operation of thermoelectric modules, one of the primary steps for module design is to use thermoelectric and interfacial materials with as close CTEs as possible. Compared with that of Fe and Ni contact layers, the CTE of Mg_2Cu is much closer to that of

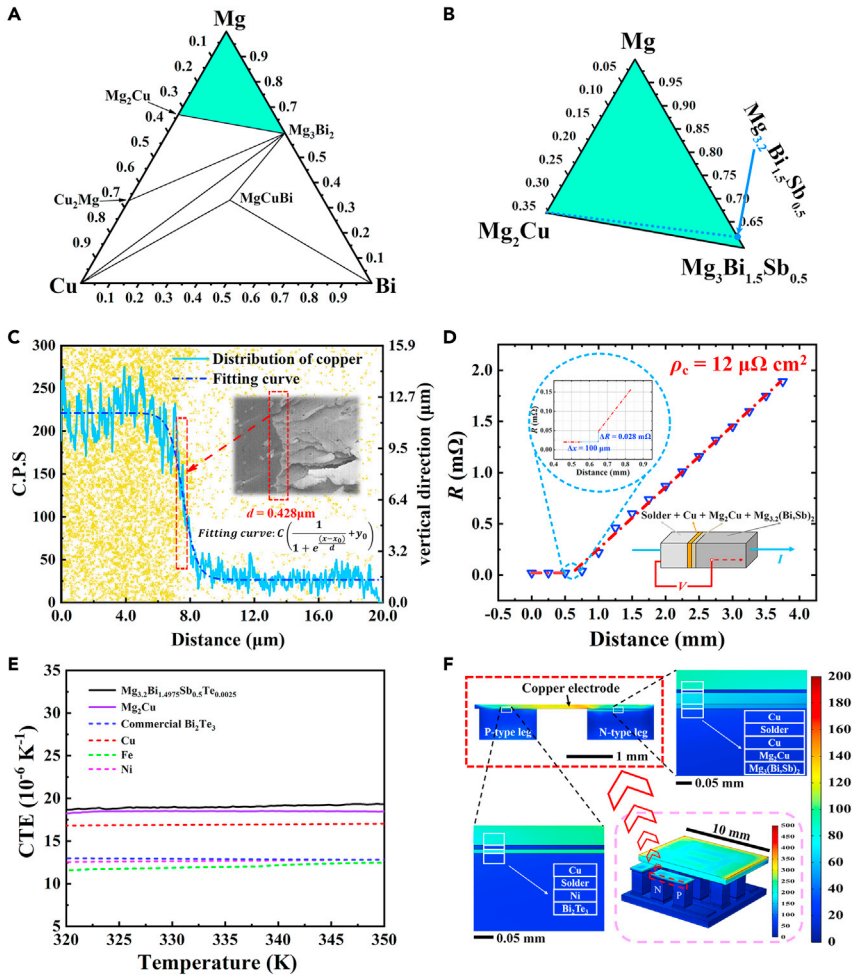

Figure 3. Property characterization of Mg_2Cu-based barrier layer material

(A and B) (A) Mg–Cu–Bi ternary phase diagrams and (B) Mg–Mg_2Cu–$Mg_3Bi_{1.5}Sb_{0.5}$ three-phase region at room temperature.

(C) Distribution of Cu near the boundary of Mg_2Cu and $Mg_{3.2}Bi_{1.4975}Sb_{0.5}Te_{0.0025}$. SEM image of the selected boundary area is shown in the inset.

(D) Contact resistance measurement of the interfacial layers.

(E) CTEs as functions of temperature for all the relevant materials in both types of modules studied in this work.

(F) Simulated thermal stress distribution near the contact layers of the module under operating conditions.

$Mg_{3.2}Bi_{1.4975}Sb_{0.5}Te_{0.0025}$. Thus, a lower thermal stress could be predicted (Figure 3E). The finite element analysis of the thermal stress distribution across the module under the conditions of fixed temperature difference and optimized current is presented in Figure 3F. In thermoelectric cooling modules, Cu is the most commonly used electrode. In our case, the CTE of Cu was much closer to that of $Mg_{3.2}Bi_{1.4975}Sb_{0.5}Te_{0.0025}$ than that of Bi_2Te_3. Meanwhile, the CTE of Mg_2Cu was in between $Mg_{3.2}Bi_{1.4975}Sb_{0.5}Te_{0.0025}$ and Cu; thus, the material acted as an ideal buffer layer to reduce the thermal stress. Our simulation clearly showed that the maximum thermal stress in the contact layer of Cu/Mg_2Cu/$Mg_{3.2}Bi_{1.4975}Sb_{0.5}Te_{0.0025}$ (70 MPa) was much lower than that in its p-type counterpart Ni/$(Sb_{0.75}Bi_{0.25})_2(Te_{0.97}Se_{0.03})_3$ (130 MPa) and that in Ni/$Mg_{3.2}Bi_{1.4975}Sb_{0.5}Te_{0.0025}$ (170 MPa) because of the newly designed structure (Figures 3F and S14). To conclude, the high stability, low contact resistance, and compensated CTE of Mg_2Cu play fundamental roles in

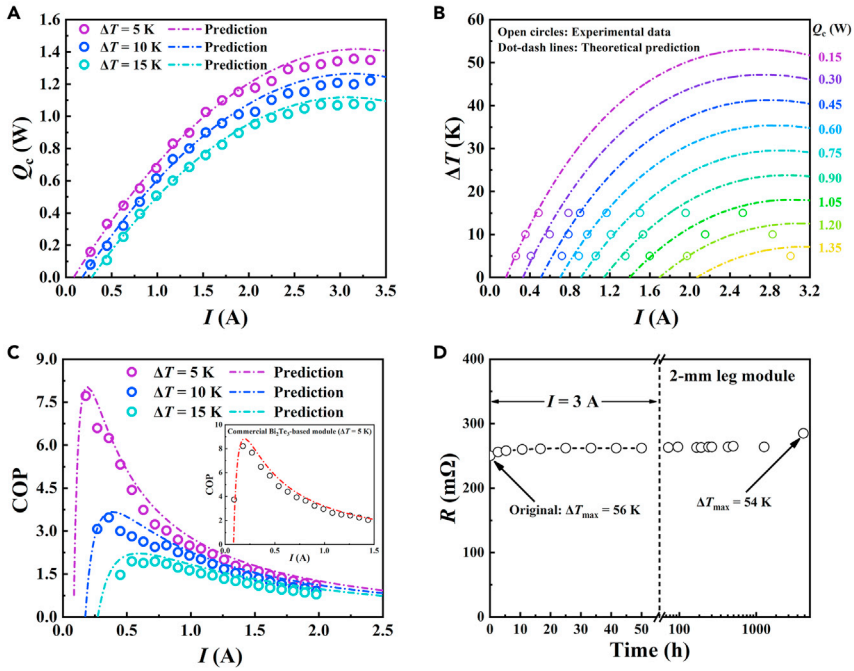

Figure 4. Cooling performance of MBST/SBTS modules

(A) Cooling power of the 7-pair module with leg length of 2 mm as a function of current.

(B) ΔT of the module (2-mm leg length) as a function of current with a fixed heat flow.

(C) COP for the 7-pair module with 2-mm legs working at various ΔT of 5, 10, and 15 K. The dotted-dashed lines represent the theoretical predictions. The inset of Figure 1D shows the COP of the commercial Bi_2Te_3-based module for comparison.

(D) Resistance of the 7-pair module with 2-mm legs was monitored for 3,000 min under the continuous current of 3 A, and after that the resistance of the module was periodically measured for about 6 months indicating the module's high durability. All the empty circles in the images represent the experimental data while the dotted-dashed lines represent the theoretical simulation.

the high-performance durable MBST/SBTS cooling modules. This proved the superior advantage of the Mg_2Cu barrier layer over that of Ni/Fe in the fabrication of commercially viable full-scale $Mg_3(Bi,Sb)_2$-based cooling modules. Indeed, this principle paves the way to fabricate other near room temperature high-performance thermoelectric modules, such as for the SnSe-based materials.[45]

We aimed to obtain more details of cooling performance of the MBST/SBTS modules to facilitate their possibility of commercial application. The cooling capacity (Q_c), which is the heat absorbed by the cold side of the module, was measured for 7 pairs of modules with 2mm thick legs. As observed in Figure 4A, the cooling heat flow increased with the current and gradually reached the maximum cooling capacity (Q_{cmax}). With small ΔT between the two sides of the module, a large cooling capacity was produced by the thermoelectric module because of the less cooling heat dissipated by thermal conduct in the materials. As ΔT increases from 5 to 15 K, Q_{cmax} corresponding to various ΔT decreases from 1.4 to 1.1 W with the optimal current being ~3.2 A (Figure 4A). Meanwhile, identical Q_{cmax} (1.5 W) was obtained for the 7-pair and 2-mm-leg Bi_2Te_3-based module under similar measurement conditions (ΔT = 5 K, current = 3.5 A) shown in Figure S3. ΔT, which the cooling module could provide with different heat loads, was calculated (Figure 4B) and used to predict the cooling performance of the MBST/SBTS modules under specific working

conditions. ΔT_{max} decreased with the increase of the cooling heat flow at a rate of ~35 K W^{-1}, which is in good agreement with the theoretical predictions.

The energy efficiency of a refrigeration system can be characterized by the COP (COP = Q_c/W), which is another key parameter of cooling modules and is defined as the ratio between Q_c and the energy consumed (W). Cooling efficiency could be maximized with better thermoelectric materials, low temperature differences, and optimized current. As shown in Figure 4C, the maximum COP increased from ~2 (ΔT = 15 K) to ~7.8 (ΔT = 5 K), which is quite close to the maximum COP of 8.2 (ΔT = 5 K) for the module prepared using commercial Bi_2Te_3 legs (inset of Figure 4C). In addition, the MBST/SBTS cooling module in this work exhibited robust durability, as shown in Figure 4D. The resistance of the 7-pair module was nearly constant after 3,000 min of operation under a continuous current of 3 A, and the increase of the total resistance was within 5%. After that, the module was monitored for about 6 months with the resistance periodically measured as shown in Figure 4D. The stability of performance after 6 months is comparable to that of the commercial Bi_2Te_3-based modules.[53]

In conclusion, full-scale MBST/SBTS thermoelectric cooling modules (7, 31, and 71 pairs) with a 23% higher performance-cost ratio to that of the commercial Bi_2Te_3 modules were demonstrated in this work. Owing to the high thermoelectric performance and enhanced stability of the n-type $Mg_{3.2}Bi_{1.4975}Sb_{0.5}Te_{0.0025}$ material, low contact resistance, and low thermal stress of the Mg_2Cu-based interfacial layer, superior thermoelectric cooling performance, and service durability were realized in our modules. Given that the manufacturing process of the MBST/SBTS modules is compatible with other high-performance $Mg_3(Bi,Sb)_2$ samples prepared by different methods, we can rationally envision that the cooling performance of new module based on improved near room temperature zTs of the $Mg_3(Bi,Sb)_2$ materials would be further enhanced. This work has solved the practical issues of MBST/SBTS-based modules and paves the road for its application in the next-generation thermoelectric cooling techniques.

EXPERIMENTAL PROCEDURES

Resource availability

Lead contact

Further information and requests for resources and materials should be directed to and will be fulfilled by the lead contact, Huaizhou Zhao (hzhao@iphy.ac.cn).

Materials availability

The materials in this study will be made available on request.

Data and code availability

The published article includes all data generated or analyzed during this study.

Full experimental procedures are provided in the supplemental information.

SUPPLEMENTAL INFORMATION

Supplemental information can be found online at https://doi.org/10.1016/j.joule.2021.11.008.

ACKNOWLEDGMENTS

The authors acknowledge the funding support from The National Key Research and Development Program of China under the grant number of 2018YFA0702100. This

work is supported by the Center for Clean Energy, the Center for Materials Genome, and the Synergic Extreme Condition User Facility. We would like to acknowledge the valuable contribution to this work made by Guijun Chi, Zongxiang Kan, and Shushan Chen of Xianghe oriental electronic, and thank Dr. Baoan Sun for the measurement of CTE.

AUTHOR CONTRIBUTIONS

Conceptualization, H.Z.; methodology, H.Z., H.Z., and G.L.; investigation, J.Y., J.G., N.C., T.L., J.X., and Y.Y.; writing – original draft, H.Z. and J.Y.; writing – review & editing, H.Z., H.Z., G.L., and R.Y.; funding acquisition, H.Z.; resources, H.Z., P.S., and L.G.; and supervision, H.Z. and H.Z.

DECLARATION OF INTERESTS

H.Z., J.Y., and J.G. have filed one Patent Cooperation Treaty patent application (PCT201910811895.X) on the work described here.

Received: October 6, 2021
Revised: October 25, 2021
Accepted: November 19, 2021
Published: December 14, 2021

REFERENCES

1. Mao, J., Liu, Z.H., Zhou, J.W., Zhu, H.T., Zhang, Q., Chen, G., and Ren, Z.F. (2018). Advances in thermoelectrics. Adv. Phys. *67*, 69–147. https://doi.org/10.1080/00018732.2018.1551715.

2. Zhang, J.W., Song, L.R., Borup, K.A., Jørgensen, M.R.V., and Iversen, B.B. (2018). New insight on tuning electrical transport properties via chalcogen doping in n-type Mg3Sb2-based thermoelectric materials. Adv. Energy Mater. *8*, 1702776. https://doi.org/10.1002/aenm.201702776.

3. Heremans, J.P., Jovovic, V., Toberer, E.S., Saramat, A., Kurosaki, K., Charoenphakdee, A., Yamanaka, S., and Snyder, G.J. (2008). Enhancement of thermoelectric efficiency in PbTe by distortion of the electronic density of states. Science *321*, 554–557. https://doi.org/10.1126/science.1159725.

4. Pei, Y.Z., Shi, X.Y., LaLonde, A., Wang, H., Chen, L.D., and Snyder, G.J. (2011). Convergence of electronic bands for high performance bulk thermoelectrics. Nature *473*, 66–69. https://doi.org/10.1038/nature09996.

5. Tang, Y.L., Gibbs, Z.M., Agapito, L.A., Li, G., Kim, H.S., Nardelli, M.B., Curtarolo, S., and Snyder, G.J. (2015). Convergence of multi-valley bands as the electronic origin of high thermoelectric performance in CoSb3 skutterudites. Nat. Mater. *14*, 1223–1228. https://doi.org/10.1038/nmat4430.

6. Mao, J., Shuai, J., Song, S.W., Wu, Y.X., Dally, R., Zhou, J.W., Liu, Z.H., Sun, J.F., Zhang, Q.Y., Dela Cruz, C., et al. (2017). Manipulation of ionized impurity scattering for achieving high thermoelectric performance in n-type Mg3Sb2-based materials. Proc. Natl. Acad. Sci. USA *114*, 10548–10553. https://doi.org/10.1073/pnas.1711725114.

7. Shuai, J., Mao, J., Song, S.W., Zhu, Q., Sun, J.F., Wang, Y.M., He, R., Zhou, J.W., Chen, G., Singh, D.J., and Ren, Z.F. (2017). Tuning the carrier scattering mechanism to effectively improve the thermoelectric properties. Energy Environ. Sci. *10*, 799–807. https://doi.org/10.1039/c7ee00098g.

8. Kuo, J.J., Kang, S.D., Imasato, K., Tamaki, H., Ohno, S., Kanno, T., and Snyder, G.J. (2018). Grain boundary dominated charge transport in Mg3Sb2-based compounds. Energy Environ. Sci. *11*, 429–434. https://doi.org/10.1039/c7ee03326e.

9. Tritt, T.M. (1999). Thermoelectric materials—holey and unholey semiconductors. Science *283*, 804–805. https://doi.org/10.1126/science.283.5403.804.

10. Zhao, L.D., Lo, S.H., Zhang, Y.S., Sun, H., Tan, G.J., Uher, C., Wolverton, C., Dravid, V.P., and Kanatzidis, M.G. (2014). Ultralow thermal conductivity and high thermoelectric figure of merit in SnSe crystals. Nature *508*, 373–377. https://doi.org/10.1038/nature13184.

11. Zhao, L.D., He, J.Q., Berardan, D., Lin, Y.H., Li, J.F., Nan, C.W., and Dragoe, N. (2014). BiCuSeO oxyselenides: new promising thermoelectric materials. Energy Environ. Sci. *7*, 2900–2924. https://doi.org/10.1039/c4ee00997e.

12. Liu, Z.H., Zhang, W.H., Gao, W.H., and Mori, T. (2021). A material catalogue with glass-like thermal conductivity mediated by crystallographic occupancy for thermoelectric application. Energy Environ. Sci. *14*, 3579–3587. https://doi.org/10.1039/d1ee00738f.

13. Liu, H.L., Shi, X., Xu, F.F., Zhang, L.L., Zhang, W.Q., Chen, L.D., Li, Q., Uher, C., Day, T., and Snyder, G.J. (2012). Copper ion liquid-like thermoelectrics. Nat. Mater. *11*, 422–425. https://doi.org/10.1038/nmat3273.

14. Poudel, B., Hao, Q., Ma, Y., Lan, Y.C., Minnich, A., Yu, B., Yan, X.A., Wang, D.Z., Muto, A., Vashaee, D., et al. (2008). High-thermoelectric performance of nanostructured bismuth antimony telluride bulk alloys. Science *320*, 634–638. https://doi.org/10.1126/science.1156446.

15. Biswas, K., He, J.Q., Blum, I.D., Wu, C.I., Hogan, T.P., Seidman, D.N., Dravid, V.P., and Kanatzidis, M.G. (2012). High-performance bulk thermoelectrics with all-scale hierarchical architectures. Nature *489*, 414–418. https://doi.org/10.1038/nature11439.

16. Zhao, W., Liu, Z., Sun, Z., Zhang, Q.J., Wei, P., Mu, X., Zhou, H., Li, C., Ma, S., He, D., et al. (2017). Superparamagnetic enhancement of thermoelectric performance. Nature *549*, 247–251. https://doi.org/10.1038/nature23667.

17. Qin, C., Cheng, L., Xiao, Y., Wen, C., Ge, B., Li, W., and Pei, Y. (2021). Substitutions and dislocations enabled extraordinary n-type thermoelectric PbTe. Mater. Today Phys. *17*, 100355. https://doi.org/10.1016/j.mtphys.2021.100355.

18. Wu, Y., Chen, Z., Nan, P., Xiong, F., Lin, S., Zhang, X., Chen, Y., Chen, L., Ge, B., and Pei, Y. (2019). Lattice strain advances thermoelectrics. Joule *3*, 1276–1288. https://doi.org/10.1016/j.joule.2019.02.008.

19. Kim, S.I., Lee, K.H., Mun, H.A., Kim, H.S., Hwang, S.W., Roh, J.W., Yang, D.J., Shin, W.H., Li, X.S., Lee, Y.H., et al. (2015). Dense dislocation arrays embedded in grain boundaries for high-performance bulk thermoelectrics. Science *348*, 109–114. https://doi.org/10.1126/science.aaa4166.

20. Bell, L.E. (2008). Cooling, heating, generating power, and recovering waste heat with thermoelectric systems. Science *321*, 1457–

1461. https://doi.org/10.1126/science.1158899.

21. Li, J., Zhang, S., Jia, F., Zheng, S.Q., Shi, X.L., Jiang, D.Q., Wang, S.Y., Lu, G.W., Wu, L.M., and Chen, Z.G. (2020). Point defect engineering and machinability in n-type Mg3Sb2-based materials. Mater. Today Phys. *15*, 100269. https://doi.org/10.1016/j.mtphys.2020.100269.

22. Jørgensen, L.R., Zhang, J.W., Zeuthen, C.B., and Iversen, B.B. (2018). Thermal stability of Mg3Sb1.475Bi0.475Te0.05 high performance n-type thermoelectric investigated through powder X-ray diffraction and pair distribution function analysis. J. Mater. Chem. A *6*, 17171–17176. https://doi.org/10.1039/c8ta06544f.

23. Qiu, P., Mao, T., Huang, Z., Xia, X., Liao, J., Agne, M., Gu, M., Zhang, Q., Ren, D., Bai, S., et al. (2019). High-efficiency and stable thermoelectric module based on liquid-like materials. Joule *3*, 1538–1548. https://doi.org/10.1016/j.joule.2019.04.010.

24. Yin, L., Chen, C., Zhang, F., Li, X., Bai, F., Zhang, Z., Wang, X., Mao, J., Cao, F., Chen, X., et al. (2020). Reliable N-type Mg3.2Sb1.5Bi0.49Te0.01/304 stainless steel junction for thermoelectric applications. Acta Mater *198*, 25–34. https://doi.org/10.1016/j.actamat.2020.07.058.

25. Liu, W.S., Wang, H.Z., Wang, L.J., Wang, X.W., Joshi, G., Chen, G., and Ren, Z.F. (2013). Understanding of the contact of nanostructured thermoelectric n-type Bi2Te2.7Se0.3 legs for power generation applications. J. Mater. Chem. A *1*, 13093–13100. https://doi.org/10.1039/c3ta13456c.

26. Vining, C.B. (2009). An inconvenient truth about thermoelectrics. Nat. Mater. *8*, 83–85. https://doi.org/10.1038/nmat2361.

27. Chung, D.Y., Hogan, T., Brazis, P., Rocci-Lane, M., Kannewurf, C., Bastea, M., Uher, C., and Kanatzidis, M.G. (2000). CsBi4Te6: a high-performance thermoelectric material for low-temperature applications. Science *287*, 1024–1027. https://doi.org/10.1126/science.287.5455.1024.

28. Venkatasubramanian, R., Siivola, E., Colpitts, T., and O'Quinn, B. (2001). Thin-film thermoelectric devices with high room-temperature figures of merit. Nature *413*, 597–602. https://doi.org/10.1038/35098012.

29. Harman, T.C., Taylor, P.J., Walsh, M.P., and LaForge, B.E. (2002). Quantum dot superlattice thermoelectric materials and devices. Science *297*, 2229–2232. https://doi.org/10.1126/science.1072886.

30. DiSalvo, F.J. (1999). Thermoelectric cooling and power generation. Science *285*, 703–706. https://doi.org/10.1126/science.285.5428.703.

31. Liu, Z., Sato, N., Gao, W.H., Yubuta, K., Kawamoto, N., Mitome, M., Kurashima, K., Owada, Y., Nagase, K., Lee, C.H., et al. (2021). Demonstration of ultrahigh thermoelectric efficiency of ~7.3% in Mg3Sb2/MgAgSb module for low-temperature energy harvesting. Joule *5*, 1196–1208. https://doi.org/10.1016/j.joule.2021.03.017.

32. Chen, X.X., Wu, H.J., Cui, J., Xiao, Y., Zhang, Y., He, J.Q., Chen, Y., Cao, J., Cai, W., Pennycook, S.J., et al. (2018). Extraordinary thermoelectric performance in n-type manganese doped Mg3Sb2 Zintl: high band degeneracy, tuned carrier scattering mechanism and hierarchical microstructure. Nano Energy *52*, 246–255. https://doi.org/10.1016/j.nanoen.2018.07.059.

33. Mao, J., Zhu, H.T., Ding, Z.W., Liu, Z.H., Gamage, G.A., Chen, G., and Ren, Z.F. (2019). High thermoelectric cooling performance of n-type Mg3Bi2-based materials. Science *365*, 495–498. https://doi.org/10.1126/science.aax7792.

34. Shu, R., Zhou, Y.C., Wang, Q., Han, Z.J., Zhu, Y.B., Liu, Y., Chen, Y.X., Gu, M., Xu, W., Wang, Y., et al. (2019). Mg3+δSbxBi2−x family: a promising substitute for the state-of-the-art n-type thermoelectric materials near room temperature. Adv. Funct. Mater. *29*, 1807235. https://doi.org/10.1002/adfm.201807235.

35. Zhang, J., Song, L., Pedersen, S.H., Yin, H., Hung, L.T., and Iversen, B.B. (2017). Discovery of high-performance low-cost n-type Mg3Sb2-based thermoelectric materials with multi-valley conduction bands. Nat. Commun. *8*, 13901. https://doi.org/10.1038/ncomms13901.

36. Tamaki, H., Sato, H.K., and Kanno, T. (2016). Isotropic conduction network and defect chemistry in Mg3+δSb2-based layered Zintl compounds with high thermoelectric performance. Adv. Mater. *28*, 10182–10187. https://doi.org/10.1002/adma.201603955.

37. Imasato, K., Kang, S.D., and Snyder, G.J. (2019). Exceptional thermoelectric performance in Mg3Sb0.6Bi1.4 for low-grade waste heat recovery. Energy Environ. Sci. *12*, 965–971. https://doi.org/10.1039/c8ee03374a.

38. Shi, X.M., Zhang, X.Y., Ganose, A., Park, J., Sun, C., Chen, Z.W., Lin, S.Q., Li, W., Jain, A., and Pei, Y.Z. (2021). Compromise between band structure and phonon scattering in efficient n-Mg3Sb2-Bi thermoelectrics. Mater. Today Phys. *18*, 100362. https://doi.org/10.1016/j.mtphys.2021.100362.

39. Song, S.W., Mao, J., Bordelon, M., He, R., Wang, Y.M., Shuai, J., Sun, J.Y., Lei, X.B., Ren, Z.S., Chen, S., et al. (2019). Joint effect of magnesium and yttrium on enhancing thermoelectric properties of n-type Zintl Mg3+deltaY0.02Sb1.5Bi0.5. Mater. Today Phys. *8*, 25–33. https://doi.org/10.1016/j.mtphys.2018.12.004.

40. Pan, Y., Yao, M., Hong, X., Zhu, Y., Fan, F., Imasato, K., He, Y., Hess, C., Fink, J., Yang, J., et al. (2020). Mg3(Bi,Sb)2 single crystals towards high thermoelectric performance. Energy Environ. Sci. *13*, 1717–1724. https://doi.org/10.1039/d0ee00838a.

41. Luo, T., Kuo, J.J., Griffith, K.J., Imasato, K., Cojocaru-Mirédin, O., Wuttig, M., Gault, B., Yu, Y., and Snyder, G.J. (2021). Nb-mediated grain growth and grain-boundary engineering in Mg3Sb2-based thermoelectric materials. Adv. Funct. Mater. *31*, 2100258. https://doi.org/10.1002/adfm.202100258.

42. Wood, M., Kuo, J.J., Imasato, K., and Snyder, G.J. (2019). Improvement of low-temperature zT in a Mg3Sb2-Mg3Bi2 solid solution via Mg-vapor annealing. Adv. Mater. *31*, 1902337. https://doi.org/10.1002/adma.201902337.

43. Ying, P.J., He, R., Mao, J., Zhang, Q.H., Reith, H., Sui, J.H., Ren, Z.F., Nielsch, K., and Schierning, G. (2021). Towards tellurium-free thermoelectric modules for power generation from low-grade heat. Nat. Commun. *12*, 1121. https://doi.org/10.1038/s41467-021-21391-1.

44. Shi, X.M., Sun, C., Zhang, X.Y., Chen, Z.W., Lin, S.Q., Li, W., and Pei, Y.Z. (2019). Efficient Sc-doped Mg3.05–xScxSbBi thermoelectrics near room temperature. Chem. Mater. *31*, 8987–8994. https://doi.org/10.1021/acs.chemmater.9b03156.

45. Qin, B.C., Wang, D.Y., Liu, X.X., Qin, Y.X., Dong, J.F., Luo, J.F., Li, J.W., Liu, W., Tan, G.J., Tang, X.F., et al. (2021). Power generation and thermoelectric cooling enabled by momentum and energy multiband alignments. Science *373*, 556–561. https://doi.org/10.1126/science.abi8668.

46. Rogl, G., and Rogl, P. (2017). Skutterudites, a most promising group of thermoelectric materials. Curr. Opin. Green Sustain. Chem. *4*, 50–57. https://doi.org/10.1016/j.cogsc.2017.02.006.

47. Han, Z., Gui, Z., Zhu, Y.B., Qin, P., Zhang, B.P., Zhang, W., Huang, L., and Liu, W. (2020). The electronic transport channel protection and tuning in real space to boost the thermoelectric performance of Mg3+deltaSb2−yBiy near room temperature. Research *2020*, 1672051. https://doi.org/10.34133/2020/1672051.

48. Li, A.R., Fu, C.G., Zhao, X.B., and Zhu, T.J. (2020). High-performance Mg3Sb2−xBix thermoelectrics: progress and perspective. Research *2020*, 1934848. https://doi.org/10.34133/2020/1934848.

49. Kuo, J.J., Yu, Y., Kang, S.D., Cojocaru-Mirédin, O., Wuttig, M., and Snyder, G.J. (2019). Mg deficiency in grain boundaries of n-type Mg3Sb2 identified by atom probe tomography. Adv. Mater. Interfaces *6*, 1900429. https://doi.org/10.1002/admi.201900429.

50. Garbrecht, M., Saha, B., Schroeder, J.L., Hultman, L., and Sands, T.D. (2017). Dislocation-pipe diffusion in nitride superlattices observed in direct atomic resolution. Sci. Rep. *7*, 46092. https://doi.org/10.1038/srep46092.

51. Shang, S.L., Zhou, B.C., Wang, W.Y., Ross, A.J., Liu, X.L., Hu, Y.J., Fang, H.Z., Wang, Y., and Liu, Z.K. (2016). A comprehensive first-principles study of pure elements: vacancy formation and migration energies and self-diffusion coefficients. Acta Mater *109*, 128–141. https://doi.org/10.1016/j.actamat.2016.02.031.

52. Xu, C.C., Liang, Z.X., Shang, H.J., Wang, D., Wang, H., Ding, F., Mao, J., and Ren, Z.F. (2021). Scalable synthesis of n-type Mg3Sb2-xBix for thermoelectric applications. Mater. Today Phys. *17*, 100336. https://doi.org/10.1016/j.mtphys.2020.100336.

53. Wang, C.H., Hsieh, H.C., Sun, Z.W., Ranganayakulu, V.K., Lan, T.W., Chen, Y.Y., Chang, Y.Y., and Wu, A.T. (2020). Interfacial stability in Bi2Te3 thermoelectric joints. ACS Appl. Mater. Interfaces *12*, 27001–27009. https://doi.org/10.1021/acsami.9b22853.